Journal of Applied Fluid Mechanics, Vol. 11, No. 2, pp. 361-374, 2018.
Available online at www.jafmonline.net, ISSN 1735-3572, EISSN 1735-3645.
DOI: 10.29252/jafm.11.02.28243

Optimization of Freestream Flow Effects on Thrust Shock Vector Control Nozzle

F. Forghany[1†], M. Taeibe Rahni [2] and A. Asadollahi Ghohieh [3]

[1] *Department of Mechanical and Aerospace Engineering, Science and Research Branch, Islamic Azad University, Tehran, Iran*
[2] *Department of Aerospace Engineering, Sharif University of Technology, Tehran, Iran*
[3] *Civil Aviation Technology College, Tehran, Iran*

†*Corresponding Author Email: farzad_forghany@yahoo.com*

(Received July 22, 2017; accepted November 6, 2017)

ABSTRACT

The present study attempted to utilize a computational investigation to optimize the external freestream flow influence on thrust-vector control. The external flow with different Mach numbers from 0.05 to 1.1 and with optimum injection angles from 60˚ to 120˚ were studied at variable flow conditions. Simulation of a converging-diverging nozzle with shock-vector control method was performed, using the unsteady Reynolds-averaged Navier-Stokes approach with Spalart-Allmaras turbulence model. This research established that freestream flow and fluidic-injection angle are the significant parameters on shock-vector control performance. Computational results indicate that, increasing freestream Mach number would decline the thrust vectoring effectiveness. Also, optimizing injection angle would reduce the negative effect of external freestream flow on thrust-vector control. Moreover, increasing secondary to primary total pressure ratios and decreasing nozzle pressure ratios at different freestream Mach number would decrease dynamic response of starting thrust-vector control. Additionally, to lead the improvement of the next generation of jet engine concepts, the current study aimed to originate a database of variable external flow with effective aerodynamic parameters, which have influence on fluidic thrust-vector control.

Keywords: Shock vector control; Freestream flow; Fluidic-injection angle; Dynamic response.

NOMENCLATURE

A_e	exit area of nozzle
A_t	throat area of nozzle
A_e/A_t	nozzle-expansion ratio
CFD	computational fluid dynamics
FTV	fluidic thrust-vectoring
F_x	thrust axial-component
F_y	thrust normal-component
h_t	height of throat
$\dot{m}_j$	mass-flow rate of primary flow
$\dot{m}_s$	mass-flow rate of secondary flow
M_∞	Mach number of freestream
NPR	nozzle-pressure ratio
$p_{t,j}$	total-pressure of primary flow
$p_{t,s}$	total-pressure of secondary flow
p_∞	static pressure of freestream
SPR	secondary-pressure ratio
x_t	axial location of throat
x/x_t	non dimensional x-coordinate
y^+	non dimensional first cell height
δ_p	thrust-vector angle
φ_n	normal to nozzle-surface injection angle
φ_o	optimum injection angle
η	efficiency of thrust-vector control

1. INTRODUCTION

To design a novel propulsion system, one of the main challenges is the development of an impressive power structure, which is lightweight and sufficiently strong to allow for a safe and reliable flight. Low operational cost, enhanced reliability, and achieving short landing and take-off abilities are the specifications of thrust- vector control that make it an appropriate candidate for the next generation of propulsion system. Also, thrust-vector control would enhance flight trim power and reduce trim drag during cruise. It is a very helpful vectoring capability during weak dynamic-pressure condition that flight-controlling structure loses its robustness and performance (Hanumanthrao *et al.*, 2011).

The thrust-vector control is developed to guide the aircraft movement during flight at critical velocities and post-stall high angles of attack, which are impractical flight conditions. Moreover, the thrust vectoring is employed to accompany flight-controlling surfaces to make the best use of the flight safety and agility during normal operation. The conventional techniques, depending on mechanical-hardware and the most current developing techniques that are fluidic based controlling methods are the two typical approaches applied for deflecting an engine exhaust flow up to now (Páscoa *et al.*, 2013; Abdollahzadeh *et al.*, 2015; Deere *et al.*, 2007).

The fluidic thrust-vector technology is developed as an alternative to mechanical thrust vectoring to eradicate the complications related of actuators and mechanical hardware. The fluidic thrust-vector approach dependents on employing fluidic injection without moving parts to deflect the main flow. Furthermore, comparison of the mechanical and fluidic techniques exhibits a fast response time and a minute loss in the specific impulse of thrust. The fluidic techniques present higher simplicity, stealth compatibility, reliability, and lighter weight (Cen *et al.*, 2015; Mason *et al.*, 2004). The fluidic vectoring methods were established to integrate throat skewing, synthetic jet actuators, co-flow, counter-flow, and shock-vector control (Banazadeh *et al.*, 2017; Jain *et al.*, 2015). The methods utilize fluidic-injection for thrust-vector control. Fluidic-injection into the nozzle flow functions as a barrier and cause of momentum variation (Zmijanovic *et al.*, 2012; Forghany *et al.*, 2015).

The shock-vector control technique achieves flow injection deflecting throughout oblique-shock waves produced by secondary-injection in nozzle divergent section (Jing-wei *et al.*, 2014; Zmijanovic *et al.*, 2016). This technique generally acts best at over-expanded, off-design conditions, and creates high thrust deflection angles (Kostic *et al.*, 2015; Pelt *et al.*, 2015; Neely *et al.*, 2007; Ali *et al.*, 2012). The shock-vector control method is capable of offering large deflection angle with simple configuration. However, the complications of the shock impingement is the main problem. Moreover, the deflection of the main flow from the nozzle axis due to the oblique-shock waves interact with the nozzle flow (Fig. 1).

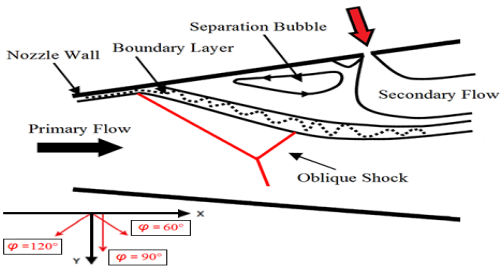

Fig. 1. Sketch of the shock vector control and injection angles with respect to nozzle axis.

The separation of boundary-layer was created by the generation gradient of the adverse-pressure due to secondary injection, where it functions as an obstacle. The oblique-shock structure creates regions of low and high pressure in the fluidic injection area and this generated shock deflects the nozzle flow. The mechanism of the shock-vector control method using oblique-shock wave is characterized by the strong gradient of adverse-pressure and with the complex structures of flows including the separation of boundary-layer, oblique-shock wave generation, oblique-shock and wake regions, and their interaction (Sellam *et al.*, 2015; Li, 2011).

The shock-vector control technique demonstrates that when secondary mass-flow is low, the fluidic injection plume is turned back and reattaches to the nozzle wall. However, when the secondary mass flow is high enough, the secondary injection plume does not reattach to the nozzle surface. In this case, the downstream area behind the fluidic injection is connected to the external freestream flow and the nozzle-pressure along the surface in the current region is relatively small (Zmijanovic *et al.*, 2012; Li, 2011).

The focus of the previous related investigations was on the two main aspects. Firstly, the study of multi-function shock-vector control (SVC) nozzle concepts, including SVC and co-flow combined concept (Chiarelli et al., 1993; Wing *et al.*, 1994), adapting SVC and mechanical vectoring concept (Anderson *et al.*, 1997), combined SVC and throat skewing concept (Federspiel *et al.*, 1995), and multi-axis thrust vectoring with convergent–divergent nozzles (Giuliano *et al.*, 1994). Secondly, the inquiry of significant parameters that would have influence on thrust vectoring include SPR, NPR, heat capacity ratio, mass-flow rate (Zmijanovic *et al.*, 2016; Guo *et al.*, 2011), injection slot shape, multi-slot injection configuration, and fluidic injection location (Kostic *et al.*, 2015; Jing-wei *et al.*, 2016; Ali *et al.*, 2012; Waithe *et al.*, 2003).

However, several important parameters on shock-vector control performance, such as optimizing of freestream flow, secondary-injection angle, and dynamic response of starting thrust vectoring were not considered. Thus, current study becomes novel and significant since numerical investigation under varied aerodynamic conditions were carried out to explore these important issues.

The current research paper was an effort to initiate a database of different external freestream flow with several effective parameter influences on fluidic thrust-vector control. The nozzle under study was a rectangular, converging-diverging with fixed fluidic-injection slot locations and nozzle-expansion ratio A_e/A_t=1.796. Simulations were executed at nozzle- pressure ratios (3.0 and 4.6), with secondary-pressure ratios (0.7 to 1.3), and different freestream Mach number (M_∞=0.05, 0.3, 0.7, and 1.1) on thrust vectoring deflection angle and efficiency of thrust-vector control. In addition, simulations were studied at optimum and normal to nozzle-surface injection angles, to understand the effect of nozzle response time during thrust vector (starting process on fluidic thrust vectoring).

In order to predict nozzle performance with external flow on thrust-vector control, the utilized injection angles at static condition (wind-off) were taken from the results obtained in our previous investigation (Forghany *et al.*, 2016). Additionally, two different comparison of the numerical and experimental results (Waithe *et al.*, 2003; Kawai *et al.*, 2007; Santiago *et al.*, 1997) were performed, for validation of our computational method.

2. COMPUTATIONAL METHODOLOGY

The PMB code (Parallel, Multi-block, Navier-Stokes, CFD code) has been developed and utilized to anticipate the nozzle-performance effects on thrust-vector control. It applies rectangular, non-axisymmetric, and convergent-divergent nozzle concept. Our explicit density-based code solved the three dimensional URANS (Unsteady Reynolds Averaged Navier-Stokes equations) with a cell-centered finite volume formulation on structured multi-block domain. It needs a structured-mesh with multi-block characteristics to let partitioning the grids into different divisions, which is important for modeling intricate structures like converging-diverging nozzle (Forghany *et al.*, 2016; Mary *et al.*, 2000; Mannini *et al.*, 2010). The unsteady RANS approach was selected for this study because it was initially capable of capturing the unsteady flow features on the starting transient process of fluidic thrust vectoring with lower computational cost than Large Eddy Simulation (LES). URANS equations were computed with Spalart-Allmaras one-equation model (Spalart *et al.*, 1992; Allmaras *et al.*, 2012).

Based on earlier researches, the Reynolds-averaged approach for fluidic thrust vectoring simulation have shown to be popular for different turbulence models such as k-ε, k-ω, and Spalart-Allmaras (Kostic *et al.*, 2015; Zmijanovic *et al.*, 2016; Deng *et al.*, 2015; Tian *et al.*, 2013). The Spalart-Allmaras turbulence model was utilized specifically for aerospace applications involving compressible flows, prediction of separation regions, wall bounded flows, and shock boundary-layer interactions. The Spalart-Allmaras model is the least computational cost in terms of CPU time and memory that is easy to implement for any type of grid. Moreover, this model has the transported variable gradients at the near wall lower than k-ε or k-ω models. Thus, the Spalart-Allmaras turbulence model was employed for its accuracy, reliability, robustness, and lower run time (Jing-wei *et al.*, 2016; Sellam *et al.*, 2015; Tian *et al.*, 2013; Neely *et al.*, 2007).

The Advection Upstream Splitting Method Plus (AUSM+), which is a flux-vector splitting scheme determined inviscid flux terms. The AUSM+ possesses a number of favorable characteristics, for instance offering precise resolution of shock waves with related domains, regularly resulting in a more rapid convergence rate, and existence free of fluctuations while moving shocks and stationary (Liou, 2001). The limiter of Van-Albada avoiding spurious fluctuations close to the shocks and the Monotone Upstream Central Scheme for Conservation Laws (MUSCL) interpolation was employed to attain 2nd-order accuracy in space.

The convergence criterion is considered with the initial residuals reduction larger than eight orders of magnitude. The difference between the numerical computation of nozzle inflow and outflow mass flux is needed to reach lower than 0.1%. It is obvious that a stable and consistent computation is adequate to provide a convergent steady solution, however, not able to guarantee a convergent unsteady solution. A convergent transient solution might be achieved by acceptable reduction of time steps size (Yao, 2012; Yao *et al.*, 2008). Accordingly, the computational time-step was obtained 8.6×10^{-9} sec. Moreover, an explicit 4th-order scheme of Runge-Kutta for integration of time was utilized in all blocks. Furthermore, the viscous terms were discretized by second-order central difference approximation (Birken, 2012).

In this research, the nozzle from NASA LaRC (Waithe *et al.*, 2003) including three-dimensional, rectangular, non-axisymmetric, and convergent-divergent structure was utilized. The nozzle length was 115.6 mm, while distance from inlet to throat was 57.8 mm. Moreover, the nozzle throat area was 2785.2 mm² and the throat height was 27.5 mm. The fluidic injection port were positioned at 46.35 mm from throat to fluidic-injection slot, whereas the slot width was 2.03 mm (Fig. 2).

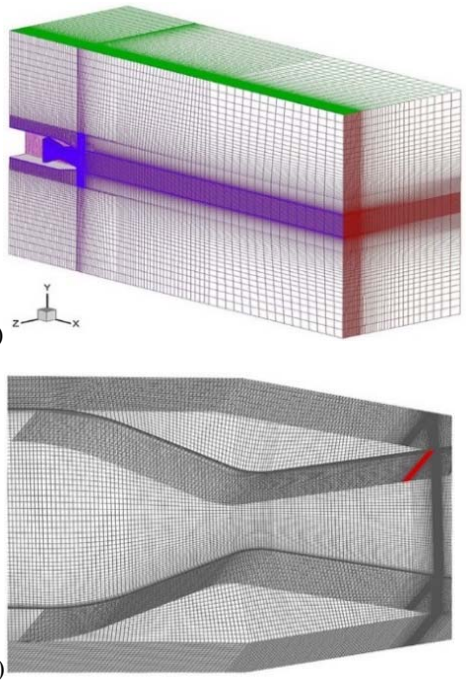

Fig. 2. The computational grid presenting: (a) Nozzle with external freestream and (b) Nozzle with fluidic-injection slot.

The stagnation conditions were defined in the primary and secondary-injection flows with a stable total-temperature (298.5 K) and total-pressure boundary condition in respect to planned nozzle-pressure ratio and secondary-pressure ratio. Furthermore, the external freestream boundaries were described with

ambient temperature and pressure conditions. In the current research, Riemann invariants were achieved along the characteristics of upstream and lateral far-field boundaries. The downstream freestream boundary was applied with a first-order extrapolation outflow condition. In addition, an adiabatic, no-slip wall condition was utilized on the nozzle walls to attain viscous solutions.

The three meshes with different spacing, which were applied comprise of the total grid cells of about 1.5×10^6 (coarse), 3.0×10^6 (medium), and 4.5×10^6 (fine), respectively. The attained results of the fine and medium nozzle meshes are similar to each other and they are more favorable than coarse mesh. The separation line situates in the similar location for two diverse meshes and the maximum difference at static pressure-distribution is around 1.0%. Therefore, to decrease the computational cost, the computations were carried out on the medium mesh (Fig. 3).

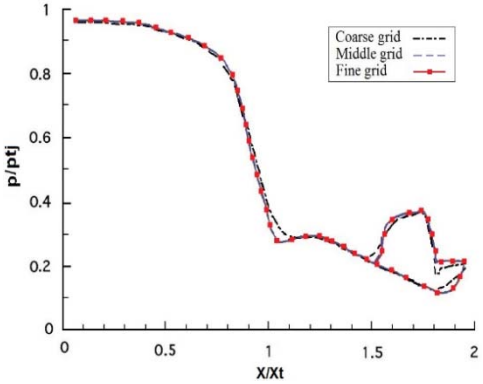

Fig. 3. Grid-independence test at SPR=0.7, NPR=4.6, and Spalart-Almaras model.

The computational domain was three-dimensional with five blocks representing the nozzle, one block defining the port of fluidic-injection, and seven blocks demonstrating the external freestream domain. The far-field were located at 34 heights of throat downstream and 8 heights of throat upstream from the nozzle outlet. The above and below of the side far-field were characterized at 25 heights of nozzle throat upper and lower than the centerline axis. The height of first grid in the wall boundary-layer was determined for $y^+<1.6$ on the fine grid.

There is a comparison between the present study's computational results and the experimental results of Waithe *et al.* (2003). Figure 4 shows, the pressure-distributions at secondary-pressure ratio of 0.7 and nozzle-pressure ratio of 4.6 with static condition (M_∞=0.1**)**. There is a notable conformity between the current computational results of pressure-distributions along the upper nozzle surface and the experimental results with a small number of inconsistencies close the oblique-shock. In the present research, the oblique-shock position at the upper wall was appeared to be x/x_t=1.49, while it was 1.61 and 1.53 in the PAB3D solver and experimental results, respectively.

Also, comparisons of stream-wise and wall-normal velocities between the numerical results of the present investigation, LES simulation results of Kawai *et al.* (2007), and the experimental results of Santiago *et al.* (1997) at the downstream region of X/D=2.0, is shown in Fig. 5.

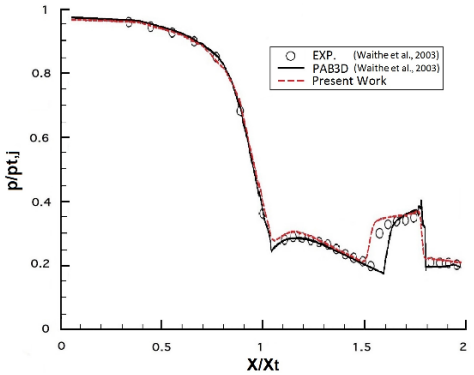

Fig. 4. Experimental and numerical pressures along upper wall of nozzle with SPR=0.7, NPR=4.6, and M_∞=0.1.

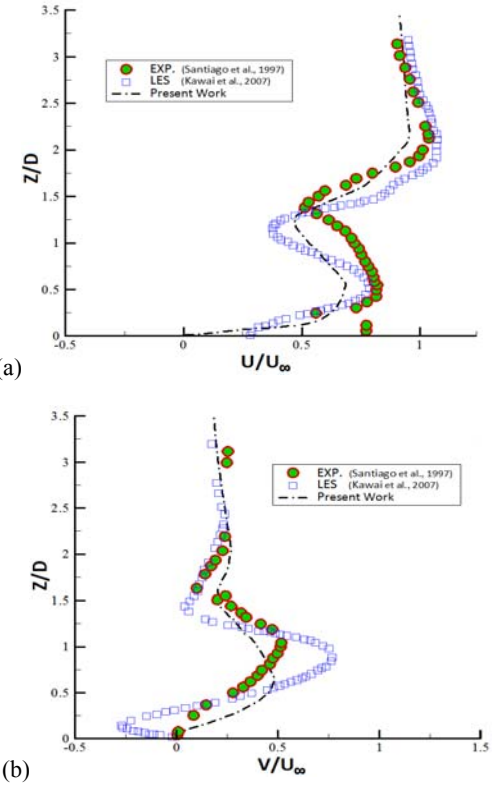

Fig. 5. Comparisons of velocities between LES, URANS, and experiment data at downstream positions of the jet of X/D = 2.0 for: (a) Stream-wise and (b) Wall-normal.

Overall, the correlation between numerical and experimental results are acceptable, apart from area close to the wall and near the jet injection exit. However, there is only a few inconsistencies between these results in the recirculating region upstream of the jet-injection. The URANS approach and LES over-predict recirculating area than the experimental results. The presence of the varied

boundary-layer upstream of the jet-injection is a justification for these discrepancies. On the other hand, the position of the shock waves and the jet injection development at downstream in this study signifies good conformity with LES and the experimental results.

3. RESULTS

In the current research, a computational study of fluidic-injection angle with different external freestream flow effects on thrust control was achieved. In order to define the thrust vector deflection angle and efficiency of thrust-vector control. Simulation of a rectangular converging-diverging nozzle with shock-vector control method was performed, utilizing unsteady RANS equations with Spalart-Allmaras turbulence model. The freestream Mach number from 0.05 to 1.1 with different flow injection angles (60° to 120°) were investigated. Moreover, simulations were achieved with essential parameters (nozzle-pressure ratio, secondary-pressure ratio, and response time) on fluidic thrust vectoring.

The next sections presents, the influence of freestream flow with fluidic-injection angle. After that, the impact of nozzle-pressure ratio, secondary-pressure ratio, and starting transient process with external freestream flow are discussed, respectively.

3.1 Effect of External Freestream flow with Secondary Injection Angle

To explain the influence of freestream flow with different flow injection angle on thrust-vector control, simulations were done at static condition (M_∞=0.05), dynamic freestream flow (M_∞=0.3, 0.7, and 1.1) and with variable fluidic-injection angles (60° to 120°). The flow condition included different secondary-pressure ratio (0.7 to 1.3), variable nozzle-pressure ratio (3.0 and 4.6), and with nozzle-expansion ratio of A_e/A_t=1.796 (Figs 6 and 7).

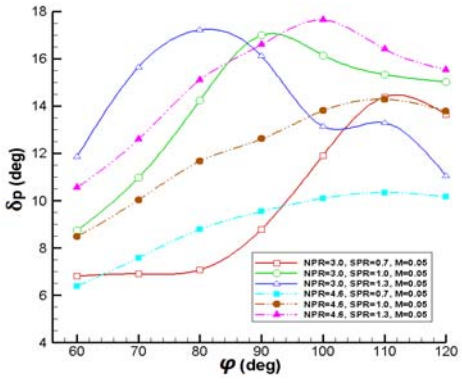

Fig. 6. Thrust-vector deflection angles at wind-off condition (M_∞=0.05) with variable SPR, NPR, and fluidic-injection angles.

Optimizing of fluidic-injection angles with reducing the nozzle mass-flow rate would make the shock and expansion waves become stronger. Moreover, the total-pressure of fluidic injection is improved as the oblique-shock and the separation of boundary-layer from the upper wall move upstream. The influence of increasing total-pressure of fluidic-injection would have positive influence on thrust-vector deflection angle and efficiency of thrust-vector control. Increasing thrust-vector deflection angle is the outcome of the increase of pressure-differential along the surfaces of nozzle.

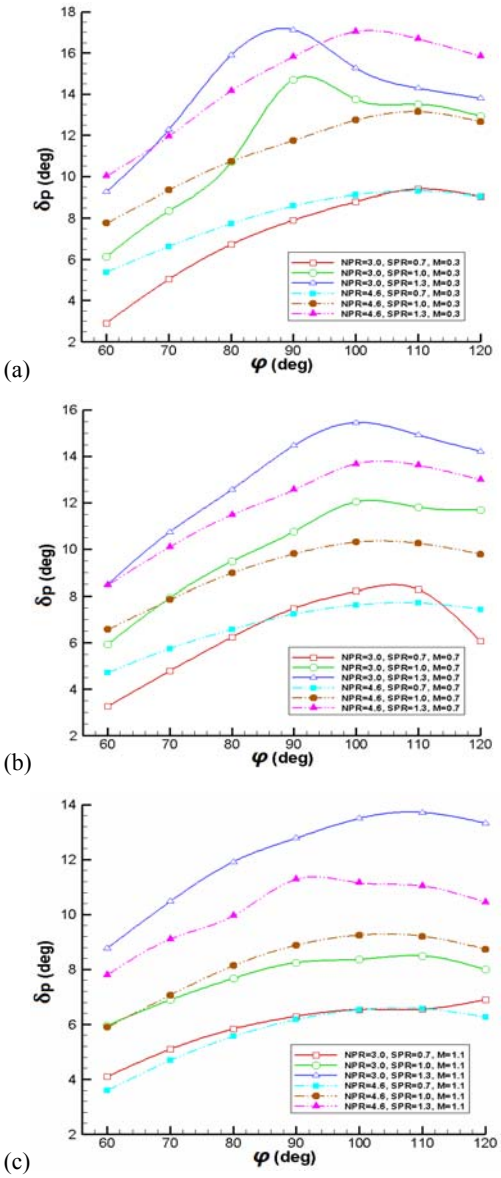

Fig. 7. Thrust-vector deflection angles at wind-on conditions with variable SPR, NPR, and fluidic-injection angles for: (a) M_∞=0.3, (b) M_∞=0.7, and (c) M_∞=1.1.

Furthermore, optimizing fluidic-injection angle, in all studied cases that were investigated, would reduce the negative influence of increasing freestream Mach number on thrust-vector control performance. The wind-on thrust vectoring at optimum fluidic-injection angle reduces the total-pressure losses from shock wave in the nozzle, improves the flow-momentum at the exit of nozzle, and controls the flow expansion along the nozzle walls by effective oblique-shock and expansion-

waves of fluidic-injection. Besides, the effect of the freestream flow is limited to oblique-shock and flow separation in the nozzle divergent section.

The thrust-vector deflection angle at nozzle–pressure ratio of 3.0, variable secondary-pressure ratio, and scheduled external flows (0.05, 0.3, 0.7, and 1.1) with optimum fluidic-injection angles compared to fluidic-injection angle with normal to nozzle surface would have average improvement of about 22.28%, 18.19%, 7.12%, and 3.63%, respectively. Besides, the thrust-vector angle at nozzle-pressure ratio of 4.6 with the same condition would have average enhancement of around 22.25%, 20.39%, 16.57%, and 14.35%, respectively.

The thrust-vector efficiency at nozzle-pressure ratio of 3.0, variable secondary-pressure ratio, and external freestream flows (M_∞=0.05, 0.3, 0.7, and 1.1) with optimum fluidic-injection angles compared to fluidic-injection angle with normal to nozzle surface would have average increase of about 23.81%, 20.71%, 7.74%, and 4.23%, respectively. Also, the thrust-vector efficiency at nozzle-pressure ratio of 4.6 with the constant condition would have average increase of about 19.88%, 29.13%, 22.18%, and 19.20%, respectively. The centerline pressure-distributions of upper surface along the nozzle at nozzle-pressure ratio of 3.0, secondary-pressure ratio of 0.7, with optimum and normal to nozzle-surface fluidic-injection angles, and with different external freestream Mach number, is shown in Fig. 8.

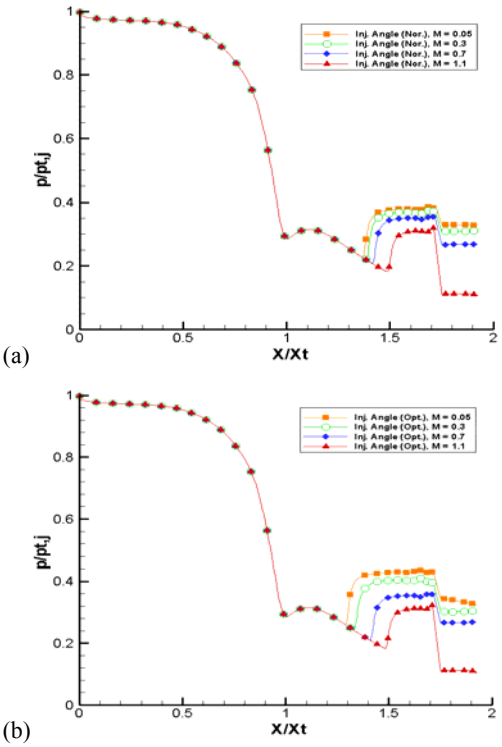

Fig. 8. Pressure-distribution of upper wall along the nozzle at SPR=0.7 and NPR=3.0 for: (a) normal to nozzle-surface injection angles and (b) optimum injection angles.

In addition, concerning the cases with nozzle-pressure ratio of 3.0, the increased pressure-differential along nozzle surfaces downstream of the injection slot by decreasing suction on the nozzle upper wall section (achieved by optimum injection angle) is slighter than the cases with nozzle-pressure ratio of 4.6, which result in higher thrust-vector angles and efficiency of thrust-vector control (with average improvements of around 26.28% and 37.48%, respectively). Mach number distributions along the nozzle at secondary-pressure ratio of 1.3, nozzle-pressure ratio of 4.6, and optimum injection angle with variable external flow, is shown in Fig. 9.

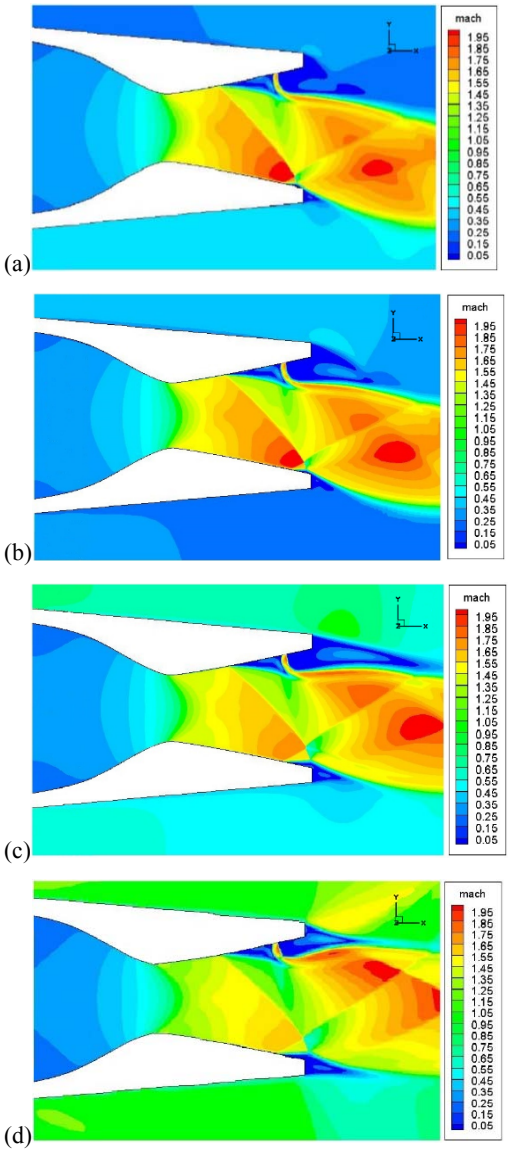

Fig. 9. Mach number distributions along the nozzle at SPR=1.3, NPR=4.6, and optimum injection angle for: (a) M_∞=0.05, (b) M_∞=0.3, (c) M_∞=0.7, and (d) M_∞=1.1.

Finally, both thrust-vector deflection angle and efficiency of thrust-vector control are under negative influence of the increasing freestream Mach number, but utilizing optimum injection angle reduces the negative effect of freestream flow

Table 1 Effect of freestream Mach number on nozzle-performance at different conditions and with optimum injection angles

Flow Condition		$M_\infty = 0.05$		$M_\infty = 0.3$		$M_\infty = 0.7$		$M_\infty = 1.1$	
NPR	SPR	δ_P (°)	η (°/%)	δ_P (°)	η (°/%)	δ_P (°)	η (°/%)	δ_P (°)	η (°/%)
3.0	0.7	14.37	3.355	8.906	2.549	6.176	1.625	5.805	1.527
	1.0	16.98	3.072	12.92	2.336	10.76	1.946	8.247	1.489
	1.3	17.20	2.324	15.89	2.147	12.56	1.697	11.92	1.611
4.6	0.7	10.32	3.099	9.291	2.787	7.698	2.309	6.569	1.971
	1.0	14.27	2.925	13.13	2.607	10.29	2.122	9.207	1.897
	1.3	17.62	2.555	17.03	2.471	13.67	1.983	11.23	1.629

Table 2 Comparisons of freestream Mach number influence on nozzle-performance between optimum and normal to nozzle-surface injection angles.

Flow Condition		$M_\infty = 0.05$		$M_\infty = 0.3$		$M_\infty = 0.7$		$M_\infty = 1.1$	
NPR	SPR	δ_P %	η %	δ_P %	η %	δ_P %	η %	δ_P %	η %
3.0	0.7	103.8	80.9	38.7	42.5	3.51	3.43	1.68	1.66
	1.0	25.7	28.4	27.1	29.7	17.2	19.8	9.61	8.21
	1.3	4.59	4.82	5.69	5.71	3.41	3.41	0.51	0.49
4.6	0.7	36.3	44.1	23.6	45.1	20.1	40.8	21.7	42.9
	1.0	27.8	48.8	25.5	41.5	17.6	37.7	15.9	35.7
	1.3	22.4	30.2	25.1	34.3	21.9	30.9	12.8	21.1

on thrust vectoring performance.

3.2 Effect of External Freestream flow with Nozzle Pressure Ratio

In order to identify the influence of freestream Mach number with different nozzle-pressure ratio on thrust-vector control, simulations were studied at static and dynamic freestream Mach numbers from 0.05 to 1.1 and with optimum and normal to nozzle-surface injection angles. The flow conditions consisted of twin nozzle-pressure ratio (3.0 and 4.6) and variable secondary-pressure ratio (0.7 to 1.3). Moreover, design-geometry limited to nozzle-expansion ratio of A_e/A_t=1.796 (Tables 1 and 2).

The comparison between the effect of dynamic freestream flow (wind-on) and static condition (wind-off) shows that increasing external freestream Mach number reduces thrust-vector deflection angle and efficiency of thrust-vector control. A larger region of separated flow under the effect of dynamic freestream flow is created when the oblique-shock wave on the lower surface moves upstream the nozzle. Moreover, the pressure along the upper wall downstream of the fluidic injection slot is influenced by external freestream flow.

In all studied cases with dynamic freestream flow, the distribution of pressure along the upper wall downstream of injection slot is lower than static pressure in ambient condition. Therefore, the static freestream condition has lower suction force on the upper wall compared to the dynamic freestream Mach number (Fig. 10).

Besides, the reduction of thrust vector effectiveness with dynamic freestream Mach number is created by the combined effects of moving oblique-shock upstream on the lower nozzle-surface and the increasing suction on the upper wall.

In most studied cases, reducing nozzle pressure ratio with decreasing freestream Mach number would have improved both thrust-vector angle and efficiency of thrust-vector control. Reducing the nozzle mass-flow rate causes the relative effectiveness of oblique-shock and expansion-waves to becoming strong and moving further upstream. The streamlines on the Mach number distributionat along the nozzle with external flow of 0.3, is shown in Fig. 11.

Furthermore, comparing cases with nozzle-pressure ratio of 3.0, the suction on the upper wall downstream of the injection slot (achieved by normal to nozzle-surface and optimum injection angles) is much greater than the cases with nozzle-pressure ratio of 4.6, resulting in greater penalty to thrust-vector deflection angles. The thrust-vector deflection angle at nozzle-pressure ratio of 3.0, variable secondary-pressure ratio, and optimum and normal to nozzle surface fluidic- injection angles with static condition (M_∞=0.05) compared to

dynamic freestream Mach numbers (0.3, 0.7, and 1.1) would have average reduction of about 11.41%, 24.52%, and 30.41%, respectively. Besides, the thrust-vector deflection angle at nozzle-pressure ratio of 4.6 with the same condition would have average decline of around 4.80%, 19.71%, and 29.51%, respectively.

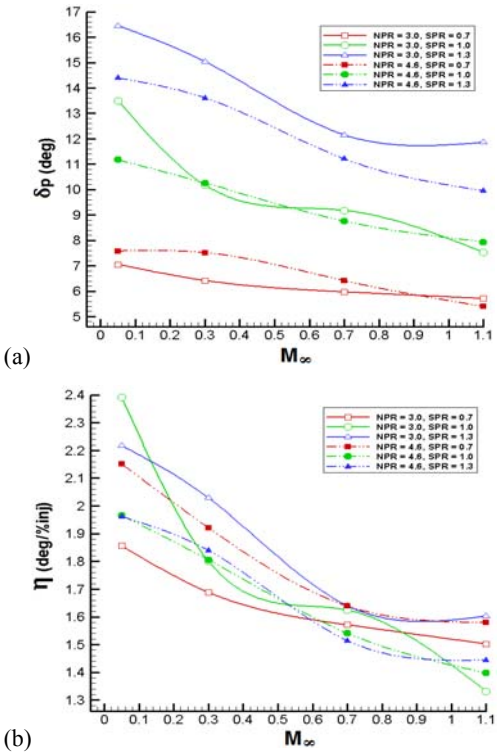

(a)

(b)

Fig. 10. Effect of Freestream flow at different NPR and SPR on: (a) Thrust-vector diflection angle and (b) thrust-vector efficiency.

The thrust-vector efficiency at nozzle-pressure ratio of 3.0, with variable secondary-pressure ratio, and with optimum and normal to nozzle surface fluidic-injection angle with wind-off condition compared to wind-on conditions (0.3, 0.7, and 1.1) would have average decrease of about 14.06%, 24.48%, and 30.36%, respectively. Also, the thrust-vector efficiency at nozzle-pressure ratio of 4.6 with equal condition would have average decline of around 8.35%, 22.72%, and 27.28%, respectively.

Moreover, in the nozzle-pressure ratio of 3.0 cases, the decreased pressure-differential along nozzle surfaces downstream of the injection slot (achieved by fluidic-injection angles) is much promising than the nozzle-pressure ratio of 4.6 cases, resulting in lower thrust-vector angles and efficiency of thrust-vector control. In addition, both thrust-vector angle and thrust-vector efficiency are under negative influence of the increasing freestream Mach number. Nevertheless, utilizing high nozzle-pressure ratio reduces the negative influence of far-field Mach number on performance of thrust vectoring.

The combined influences of reducing nozzle total-pressure due to decrease in the nozzle-pressure ratio and increasing the suction of freestream flow on the upper wall by increasing freestream Mach number would have negative effect on thrust deflection angle and efficiency of thrust vectoring. The decrease of pressure-differential along nozzle walls would result in reducing the thrust deflection angle.

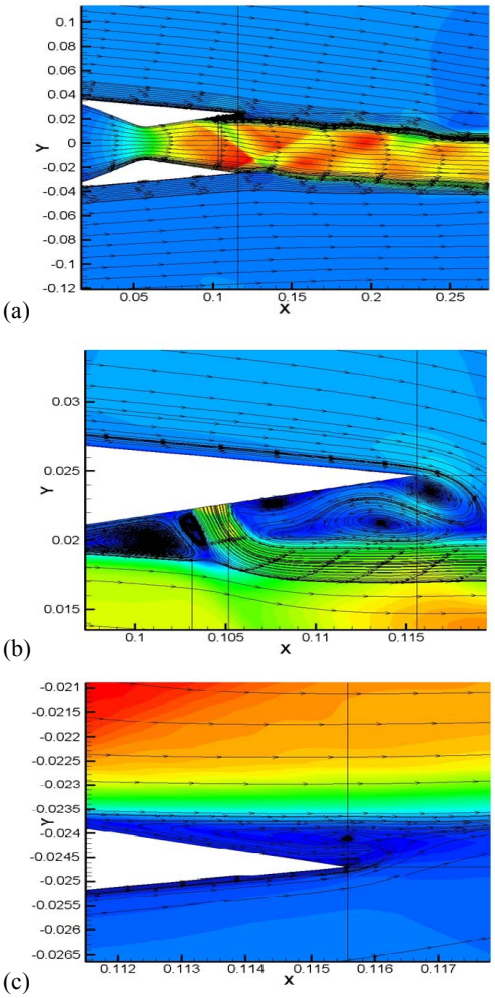

(a)

(b)

(c)

Fig. 11. Streamlines on the Mach number distributionat at M_∞=0.3, SPR=1.0, and NPR=4.6 for: (a) Far-field and nozzle, (b) Upper wall, and (c) Lower wall.

Finally, the thrust vectoring deflection angle with dynamic freestream Mach numbers compared to static condition at different secondary-pressure ratio and nozzle-pressure ratios (3.0 and 4.6) would have average decline of around 22.11% and 18.01%, respectively. Furthermore, the efficiency of thrust-vector control in the same condition would have average reduction of around 22.96% and 19.45%, respectively.

3.3 Effect of External Freestream flow with Secondary Pressure Ratio

To realize the effect of external flow with different secondary-pressure ratio on thrust-vector control, simulations were done at static and dynamic external flow from 0.05 to 1.1 and with normal to nozzle-surface and optimum injection angles. The flow condition included different secondary-

pressure ratio (0.7, 1.0, and 1.3), with variable nozzle-pressure ratio (3.0 and 4.6), and with nozzle-expansion ratio of A_e/A_t=1.796 (Tables 1 and 2).

In all studied cases, increasing secondary-nozzle ratio (SPR) at constant external freestream Mach number, increase thrust vectoring deflection angle, because the effects of oblique-shock and expansion-waves are strengthen due increase in the mass-flow rate of fluidic-injection. In addition, in most cases, increasing secondary-nozzle ratio reduces the minimum effective area in the nozzle, significantly reducing efficiency of thrust vectoring due to reducing nozzle total-pressure caused by oblique-shock and flow separation.

Once SPR is increased at unchanged far-field condition, the shock wave strength is improved and the oblique-shock shifts further upstream. Thus, when fluidic injection rate increases, pressure-distribution amplifies the improvement of the thrust-vector deflection angle. The oblique-shock and flow-separation from the lower and upper nozzle walls move upstream and reattach once more, as total-pressure of secondary injection is increased. The improvement of total-pressure of the secondary-injection flow indicates enhancement on thrust-vector deflection angle and displays decrease efficiency of thrust-vector control. This trend weakens by increasing external freestream Mach number flow. The nozzle upper wall pressure-distribution at nozzle-pressure ratio of 4.6, different secondary-pressure ratio, and variable freestream flow, is shown in Fig. 12.

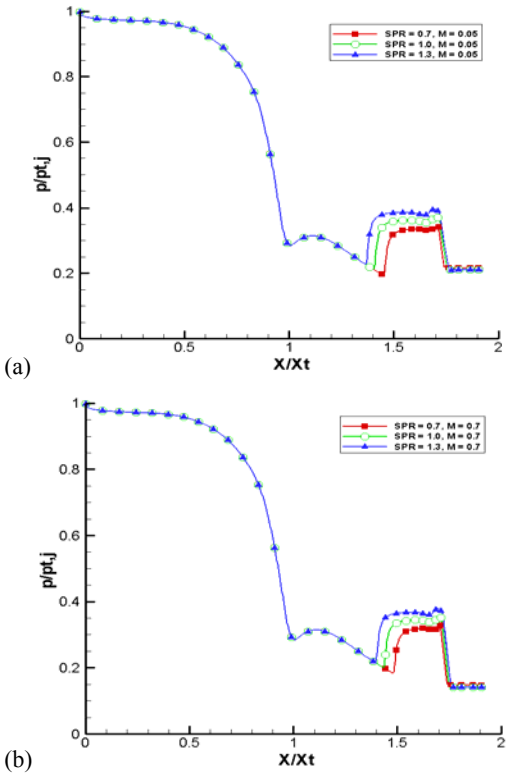

Fig. 12. Pressure-distribution of nozzle upper wall at NPR=4.6 and with different SPR for: (a) M_∞=0.05 and (b) M_∞=0.7.

Increasing freestream Mach number (wind-on) would decrease pressure-differential along nozzle surfaces resulting in the decline of thrust vectoring deflection angle. The influences of simultaneously increasing suction on the upper nozzle wall and moving the shock wave upstream on the lower wall of nozzle results in pressure-differential reduction along nozzle surfaces. Moreover, the influence of increasing total-pressure of the fluidic-injection with different freestream flow would have positive influence on the average of thrust-vector deflection angle and efficiency of thrust-vector control.

In most studied cases, increasing secondary- pressure ratio (from 0.7 to 1.3) with decreasing freestream Mach number would have improved both thrust-vector deflection angle and efficiency of thrust-vector control. Decreasing the mass-flow rate of secondary-injection reinforces the influence of oblique-shock and expansion-waves. Besides, the force and potentiality of the oblique-shock improves and the oblique-shock wave shifts upstream.

Improving secondary-pressure ratio under the effect of external freestream Mach number (wind-on), the oblique-shock wave, and flow-separation from the upper surface move upstream. Additionally, in the high SPR cases, the suction on the upper wall downstream of the injection slot (achieved by normal to nozzle-surface and optimum injection angles) is much greater than in the low SPR cases, resulting in greater penalties to thrust-vector deflection angles and efficiency of thrust-vector control.

The thrust-vector deflection angle at secondary-pressure ratio of 0.7, with different nozzle-pressure ratio (3.0 and 4.6), and with normal to nozzle-surface and optimum injection angles with static condition (M_∞=0.05) compared to dynamic freestream Mach numbers (0.3, 0.7, and 1.1) would have average reduction of about 4.92%, 15.38%, and 23.93%, respectively. Also, the thrust-vector deflection angle at secondary-pressure ratio of 1.0 with similar condition would have average decline of near 16.38%, 26.82%, and 36.59%, respectively. Besides, the thrust-vector angle at secondary-pressure ratio of 1.3 with the same condition would have average decrease of around 7.01%, 24.12%, and 29.37%, respectively.

The thrust-vector efficiency at secondary-pressure ratio of 0.7, with different nozzle-pressure ratio (3.0 and 4.6), and with normal to nozzle-surface and optimum injection angles with wind-off condition (M_∞=0.05) compared to wind-on conditions (M_∞=0.3, 0.7, and 1.1) would have average reduction of about 9.87%, 19.57%, and 22.83%, respectively. Furthermore, the thrust vectoring efficiency at secondary-pressure ratio of 1.0 with equal condition would have average decline of about 16.39%, 26.83%, and 36.61%, respectively. Additionally, the thrust-vector efficiency at secondary-pressure ratio of 1.3 with the identical condition would have average decrease of about 7.35%, 24.41%, and 27.02%, respectively.

In addition, the thrust-vector deflection angle with dynamic freestream Mach numbers compared to

static condition at different nozzle-pressure ratio and secondary-pressure ratios (0.7, 1.0, and 1.3) has average decline of about 14.75%, 26.61% and 20.17%, respectively. Also, the thrust-vector efficiency in the same condition has average reduction of about 17.42%, 26.61% and 19.59%, respectively.

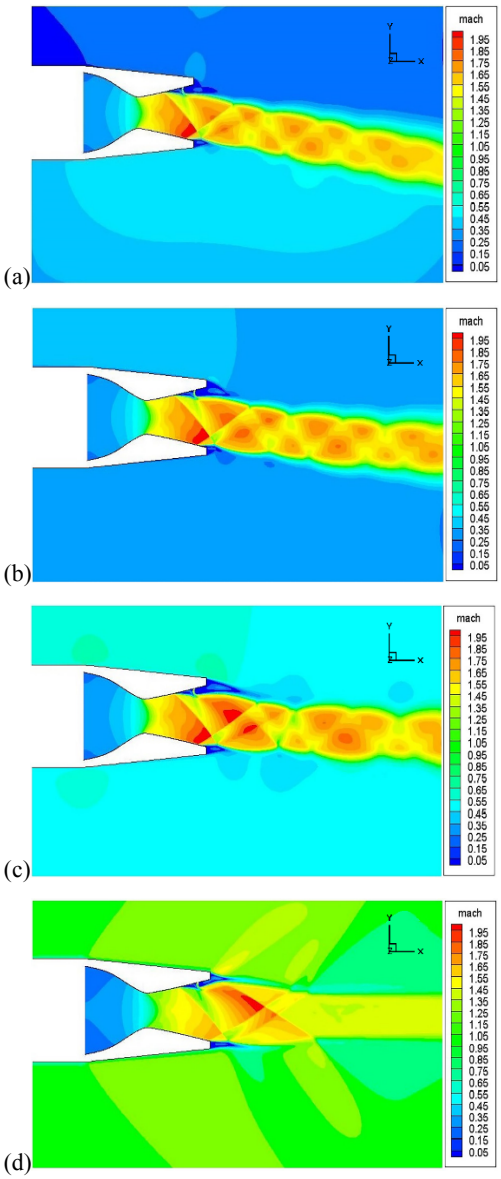

Fig. 13. Mach contours along the nozzle centerline at SPR=0.7, NPR=3.0, and normal to nozzle-surface injection angle for: (a) M_∞=0.05, (b) M_∞=0.3, (c) M_∞=0.7, and (d) M_∞=1.1.

In all studied cases with high NPR, the collective effects of reducing total-pressure of nozzle flow by decreasing secondary-pressure ratio and increasing the suction of freestream flow on the upper wall by increasing freestream Mach number would have negative effect on thrust-vector angle and efficiency of thrust-vector control. The differential pressure decrease along nozzle walls would result in reducing the thrust-vector deflection angle. The Mach contours along the nozzle and external flow at nozzle-pressure ratio of 3.0, secondary-pressure ratio of 0.7, normal to bundary fluidic-injection angle, and with different freestream Mach numbers, is shown in Fig. 13.

3.4 Effect of External Freestream flow on Starting Transient Process

The kinematics of the flow control surfaces and vectoring actuators determined the dynamic responses of mechanical thrust vectoring nozzles. Nevertheless, the dynamic response of fluidic thrust-vector control methods are not mostly clear and it depends on the case under investigation. In this research, the effects of fluidic-injection flow on dynamic response of thrust vectoring at different secondary-injection angles are studied. The pressure fluctuations through flow vectoring conditions are determined. Generally, the current simulation offered the measurement of oscillating forces, pressures, and mass-flow rates. The mass-flow rates of fluidic injection continued to be constant during the simulation. The computational solution is allowed to iterate until any fluctuations on thrust deflection angle is damped out.

To understand the effect of external flow on nozzle dynamic response during flow control (starting process of fluidic thrust vectoring), simulations were studied at static condition, dynamic external flow from 0.3 to 1.1 and with normal to nozzle-surface and optimum injection angles. The flow condition consisted of two different nozzle-pressure ratio of (3.0 and 4.6), with variable secondary-pressure ratio (1.0, 1.3, and 1.6), and with nozzle design limited to expansion ratio of A_e/A_t=1.796 (Table 3).

The achieved results indicate that in all cases, the thrust deflection angle ranges from minimum to a positive value at the initial phase of the transient process. Then, the vectoring angle recovers from positive value moves down until it approaches its highest negative value, and lastly shifts toward a stable thrust-vector angle.

In all studied cases with different freestream flow, increasing secondary-pressure ratio would improve dynamic response by increasing the influence of oblique-shock or expansion-waves. Moreover, reducing fluidic- injection angle (that is attained by normal to nozzle-surface or optimum injection angles), increases response time by decreasing the impact of secondary injection in the nozzle flow. Therefore, increasing fluidic-injection angle and secondary-pressure ratio would have positive impacts on response time during thrust-vector starting transient process.

The comparison between the effect of dynamic freestream flow (wind-on) and static condition (wind-off) demonstrates the increase of the response time (that is attained by normal to nozzle-surface or optimum injection angles) by increasing external Mach number.

Moreover, in all cases with external freestream

Table 3 Effect of different external flow on nozzle response time with normal to nozzle-surface and optimum injection angles.

Flow Condition		Response Time (ms) Optimum Injection Angles								Response Time (ms) Normal to boundary Injection			
NPR	SPR	φ_o (°)	M_∞ (.05)	φ_o (°)	M_∞ (0.3)	φ_o (°)	M_∞ (0.7)	φ_o (°)	M_∞ (1.1)	M_∞ (.05)	M_∞ (0.3)	M_∞ (0.7)	M_∞ (1.1)
3.0	1.0	90	1.36	90	1.47	100	1.51	110	1.83	1.37	1.49	1.61	1.91
	1.3	80	1.25	90	1.33	90	1.39	100	1.56	1.29	1.33	1.44	1.60
	1.6	70	1.24	70	1.25	80	1.31	90	1.39	1.22	1.21	1.34	1.47
4.6	1.0	110	1.48	110	1.58	100	1.78	90	1.90	1.56	1.69	1.80	2.14
	1.3	100	1.24	90	1.31	90	1.47	80	1.64	1.32	1.39	1.58	1.72
	1.6	90	0.93	90	0.98	80	1.03	70	1.35	0.95	1.11	1.12	1.13

flow, improving secondary-pressure ratio would reduce response time due to increase in the mass-flow rate of secondary-injection flow and improving the effectiveness of oblique-shock. Consequently, increasing mass-flow rate (achieved by increasing secondary-pressure ratio) has positive influence on dynamic response of fluidic thrust vectoring. The Effect of external flow on response time at different nozzle-pressure ratio and secondary-pressure ratio with normal to nozzle-surface and optimum fluidic-injection angles, is shown in Fig. 14.

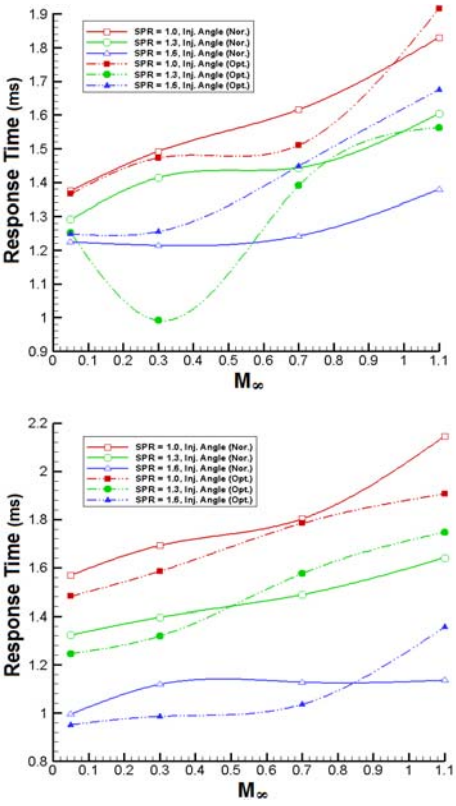

(a)

(b)

Fig. 14. Effect of freestream flow on dynamic response at different SPR with optimum and normal to nozzle-surface injection angles for: (a) NPR=3.0 (b) NPR=4.6.

Moreover, increasing nozzle-pressure ratio would increase response time due to increase in the nozzle mass-flow rate and reducing effectiveness of secondary-injection flow. The Optimum injection angles on response time at different NPR, SPR, and with variable freestream flow, is shown in Fig. 15.

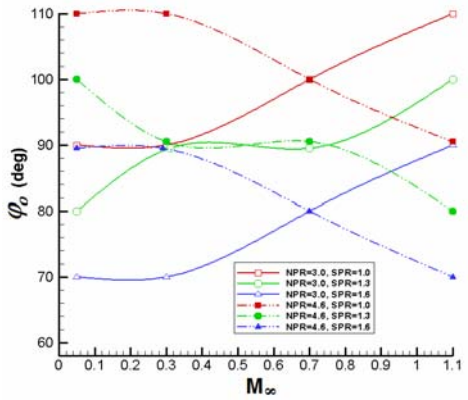

Fig. 15. Effect of freestream Mach numbers on optimum injection angles of response time at different NPR, SPR.

The dynamic response at external flow with optimum and normal to nozzle surface fluidic-injection angle, different secondary-pressure ratio and with nozzle-pressure ratio of 3.0 and 4.6 has average increase of around 13.59% and 16.11%, respectively. Thus, increasing primary mass-flow rate (achieved due to increase in the nozzle-pressure ratio) would have negative influence on dynamic response of thrust-vector control.

The optimized fluidic-injection angles, with nozzle-pressure ratio of 3.0 and secondary-pressure ratios (1.0, 1.3, and 1.6) has average increase of around 16.29%, 15.17%, and 13.87%, when the dynamic response at static condition is compared to dynamic freestream conditions. Also, the response time at nozzle-pressure ratio of 4.6 with identical condition would have average increase of around 18.34%, 19.45%, and 15.52%, respectively.

In all studied cases with increasing freestream flow and decreasing mass-flow rate (achieved by reducing nozzle-pressure ratio) would increase

response time with lowest rate at higher secondary-injection angles. Additionally, the minimum response time with increasing nozzle-pressure ratio and freestream flow is achieved at lower fluidic-injection angles.

Optimizing injection angle, in most cases that were studied, would reduce the influence of increasing freestream Mach number on dynamic response during thrust-vector starting process of fluidic thrust vectoring. Moreover, the optimized injection angles must be higher than normal to nozzle-surface injection to reduce the negative effect of increasing external flow on thrust vectoring response time.

In general, the results of dynamic response have presented more sensitivity to freestream Mach number, secondary-pressure ratio, and nozzle-pressure ratio, but less sensitivity to the fluidic-injection angle. In addition, in most cases studied, low optimum secondary-injection angles have no significant effect on dynamic response of fluidic thrust vectoring.

4. CONCLUSION

The current paper is an optimizing of freestream flow influence on fluidic thrust-vector control. The impact of essential parameters (fluidic-injection angle, nozzle-pressure ratio, secondary-pressure ratio, and dynamic response) on shock-vector control nozzle with external flows from 0.05 to 1.1 were investigated.

The findings of the study have indicated that, increasing freestream Mach number has negative influence on thrust vectoring performance. On the other hand, increasing NPR, SPR, and optimizing injection angle would decrease the negative effect of external freestream flow on thrust-vector deflection angle and efficiency of thrust-vector control (by average improvements of about 20.14% and 21.12%, respectively).

In general, increasing external freestream Mach number has negative influence on dynamic response of starting thrust vectoring. However, improving the oblique-shock effectiveness due to increasing SPR would reduce response time (with an average decline of more than 15.11%). Moreover, increasing freestream flow with decreasing mass-flow rate (achieved by reducing NPR) would increase response time with lowest rate at higher secondary-injection angles, and the best response time is achieved at high fluidic-injection angles.

REFERENCES

Abdollahzadeh, M., F. Rodrigues, J. C. Páscoa and P. J. Oliveira (2015). Numerical Design and Analysis of a Multi-DBD Actuator Configuration for the Experimental Testing of ACHEON Nozzle Model. Thrust *Aerospace Science and Technology* 41(1), 259-273.

Ali, A., G. Carlos, A. J. Neely and J. Young (2012). Combination of Thrust Modulation and Vectoring in a 2D Nozzle. *The 48th AIAA/ASME/SAE/ASEE Joint Propulsion Conference & Exhibit,* Atlanta, Georgia, AIAA Paper 2012-3780.

Allmaras, S. R., F. T. Johnson and P. R. Spalart (2012). Modifications and Clarifications for the Implementation of the Spalart-Allmaras Turbulence Model. *Seventh International Conference on Computational Fluid Dynamics*, Hawaii, ICCFD7-1902.

Anderson, C. J., V. J. Giuliano and D. J. Wing (1997). Investigation of Hybrid Fluidic/Mechanical Thrust Vectoring for Fixed Exit Exhaust Nozzle. *The 33rd Joint Propulsion Conference and Exhibit*, Seattle, WA, AIAA Paper 97-3148.

Birken, P. (2012). Optimizing Runge-Kutta Smoothers for Unsteady Flow Problems. *Electronic Transactions on Numerical Analysis* 39(1), 298-312.

Banazadeh, A. and F. Saghafi (2017). An investigation of empirical formulation and design optimization of co-flow fluidic thrust vectoring nozzles. *The Aeronautical Journal* 121(1236), 212-336.

Cen, Z., T. Smith, P. Stewart and J. Stewart (2015). Integrated Flight/Thrust Vectoring Control for Jet-powered Unmanned Aerial Vehicles with ACHEON Propulsion. *Journal of Aerospace Engineering* 229(6), 1057-1075.

Chiarelli, C. and K. Raymond (1993). Fluidic Scale Model Multi-Plane Thrust Vector Control Test Results. *The 29th AIAA/ASME/SAE/ASEE Joint Propulsion Conference & Exhibit*, Monterey, CA, AIAA Paper No. 93-2433.

Deere, K. A., J. D. Flamm, B. L. Berrier and S. K. Johnson (2007). Computational Study of an Axisymmetric Dual Throat Fluidic Thrust Vectoring Nozzle for a Supersonic Aircraft Application. *American Institute of Aeronautics and Astronautics,* AIAA Paper 2007-5085.

Deng, R. and H. D. Kim (2015). A Study on the Thrust Vector Control Using a Bypass Flow Passage. *Journal of Aerospace Engineering* 229(9), 1722-1729.

Federspiel, J. and L. Bangert (1995). Fluidic Control of Nozzle Flow-Some Performance Measurements. 95-2605.

Forghany, F., A. Asadollahi and M. Taeibe Rahni (2016). Computational study of Freestream Mach Number Effects on Fluidic Thrust Vectoring. *The 15th International Conference of Iranian Aerospace Society,* Tehran, Iran, Aero2016P82T1-3.

Forghany, F., M. Taeibe Rahni and A. Asadollahi Ghohieh (2015). Computational Investigation of Fluidic Injection Angle Effects on Thrust Vectoring. *The 16th Fluid Dynamics Conference,* Iran, FD2015-5130.

Giuliano, V. J., T. H. Flugsrad and D. J. Wing (1994). Static Investigation and Computational

Fluid Dynamics (CFD) Analysis of Flow Path Cross-Section and Trailing-Edge Shape Variations in to Multi-Axis Thrust Vectoring Nozzle Concepts. AIAA Paper No. 94-3367.

Guo, F. F., R. G. Wang and B. Zhao (2011). Effect of Variable Specific Heat on Shock Vectoring Nozzle. *Journal of Air Force Engineering University* 12(5), 15–19.

Hanumanthrao, K., S. Ragothaman, B. A. Kumar, M.G. Prasad and V. R. Sana Kumar (2011). Studies on Fluidic Injection Thrust Vectoring in Aerospike Nozzles. *49th AIAA Aerospace Sciences Meeting Including the New Horizons Forum and Aerospace Exposition*, Orlando, Florida, AIAA Paper 2011-293.

Jain, S., S. Roy, D. Gupta, V. Kumar and N. Kumar (2015). Study on Fluidic Thrust Vectoring Techniques for Application in V/STOL Aircrafts. *SAE Technical Papers,* 2015-01-2423.

Jing-wei, S., W. Zhanxue, Z. Xiao Bo, Z. Li and S. Xiao-lin (2014). Performance Estimation for Fluidic Thrust Vectoring Nozzle Coupled with Aero-engine. *The 50th AIAA/ASME/SAE/ASEE Joint Propulsion Conference*, Cleveland, OH, AIAA Paper 2014-3711.

Jingwei, S., Z. Li, W. Zhanxue and S. Xiaolin (2016). Investigation on Flow-field Characteristics and Performance of Shock Vector Control Nozzle Based on Confined Transverse Injection. *Journal of Engineering for Gas Turbines and Power 138(1), 101502.1-101502.11.*

Kawai, S. and S. K. Lele (2007). Mechanisms of Jet Mixing in a Supersonic Crossflow: a Study Using Large-eddy Simulation. *Center for Turbulence Research Annual Research Briefs.*

Kostic, O. P., Z. A. Stefanovic and I. A. Kostic (2015). CFD Modeling of Supersonic Airflow Generated by 2D Nozzle with and without an Obstacle at the Exit Section. *Journal of FME Transactions* 43(2), 107-113.

Li, L. (2011). *Numerical and Experimental Studies of Fluidic Thrust Vectoring Mechanisms*. Ph. D. thesis, Muroran Institute of Technology, Japan.

Liou, M. S. (2001). Ten Years in the Making AUSM-family. *The 5th Computational Fluid Dynamics Conference sponsored by the American Institute of Aeronautics and Astronautics*, California, AIAA Paper 2001-2521.

Mannini, C., A. Soda and G. Schewe (2010, October). Unsteady RANS Modeling of Flow past a Rectangular Cylinder, Investigation of Reynolds Number Effects. *Computers & Fluids* 39(9), 1609–1624.

Mason, M. S. and W. J. Crowther (2004). Fluidic Thrust Vectoring for Low Observable Air Vehicle. *The 2nd AIAA Flow Control Conference*, Portland, Oregon AIAA Paper 2004-2210.

Mary I., P. Sagaut and M. Deville (2000). An Algorithm for Unsteady Viscous Flows at All Speeds. *International Journal of Numerical Methods in Fluids* 34(5), 371-401.

Neely, A. J., F. N. Gesto and J. Young (2007). Performance Studies of Shock Vector Control Fluidic Thrust Vectoring. *The 43rd AIAA/ASME/SAE/ASEE Joint Propulsion Conference & Exhibit*, Cincinnati, OH, AIAA Paper 2007-5086.

Páscoa, J. C., A. Dumas, M. Trancossi, P. Stewart and D. Vucinic (2013, September). A Review of Thrust Vectoring in Support of a V/STOL Non-Moving Mechanical Propulsion System. *Central European Journal of Engineering* 3(3), 374-388.

Pelt, H. V., A. Neely and J. Young (2015). A System Study on Fluidic Thrust Vectoring. *The 20th AIAA International Space Planes and hypersonic Systems and Technologies Conferences,* Glasgow, Scotland, AIAA Paper 2015-3565.

Santiago, J. G. and J. C. Dutton (1997). Velocity Measurements of a Jet Injected into a Supersonic Crossflow. *Journal of Propulsion and Power* 13(2), 264–273.

Sellam, M., V., Zmijanovic, L. Leger, and A. Chpoun (2015). Assessment of gas thermodynamic characteristics on fluidic thrust vectoring performance: Analytical, experimental and numerical study. *International Journal of Heat and Fluid Flow* 53(1), 156–166.

Spalart, P. and S. Allmaras (1992). One-equation Turbulence Model for Aerodynamic Flows. *The 30th Aerospace Sciences Meeting and Exhibit.* Reno, NV, AIAA Paper 92-0439.

Tian, C. and L. Yijia (2013). Turbulence Models of Separated Flow in Shock Wave Thrust Vector Nozzle. *Engineering Application of Computational Fluid Mechanics* 7(2), 182-192.

Waithe, K. A. and K. A. Deere (2003). Experimental and Computational Investigation of Multiple Injection Ports in a Convergent-divergent Nozzle for Fluidic Thrust Vectoring. *21st AIAA Applied Aerodynamics Conference*, Orlando, Florida, AIAA Paper 2003-3802.

Wing, D. J. (1994). Static Investigation of Two Fluidic Thrust Vectoring Concepts on a Two-Dimensional Convergent-Divergent Nozzle. *NASA Langley Research Center,* Hampton, VA, Report No. NASA TM-4574.

Yao, L. S. (2012). Convergent Numerical Solutions of Unsteady Problems, Annual Review of Chaos Theory. *Annual Review of Chaos Theory, Bifurcations and Dynamical Systems* 2(1), 21-31.

Yao, L. S. and D., Hughes (2008). A comment on Computational periodicity as observed in a

simple system by Edward N. Lorenz. *Tellus* 60(4), 803-805.

Zmijanovic V., L. Leger and E. Depussay (2016). Experimental-Numerical Parametric Investigation of a Rocket Nozzle Secondary Injection Thrust Vectoring. *Journal of Propulsion and Power* 32(1), 196–213.

Zmijanovic V., L. Leger and V. Lago (2012). Experimental and Numerical Study of Thrust-Vectoring Effects by Transverse Gas Injection into a Propulsive Axisymmetric C-D Nozzle. *48th AIAA/ASME/SAE/ASEE Joint Propulsion Conference & Exhibit*, Atlanta, Georgia, AIAA Paper 2012-3874.